Applied Thermal Engineering 212 (2022) 118520

Contents lists available at ScienceDirect

Applied Thermal Engineering

journal homepage: www.elsevier.com/locate/apthermeng

Research Paper

Experimental characterisation of $CO_2 + C_6F_6$ mixture: Thermal stability and vapour liquid equilibrium test for its application in transcritical power cycle

G. Di Marcoberardino [a,*], E. Morosini [b], D. Di Bona [c], P. Chiesa [b], C. Invernizzi [a], P. Iora [a], G. Manzolini [b]

[a] Università degli Studi di Brescia, Dipartimento di Ingegneria Meccanica ed Industriale, via Branze, 38, 25123 Brescia, Italy
[b] Politecnico di Milano, Dipartimento di Energia, Via Lambruschini 4, 20156 Milano, Italy
[c] LEAP S.c.a r.l. - Laboratorio Energia e Ambiente Piacenza, Via Nino Bixio, 27/C, 29121 Piacenza, Italy

ARTICLE INFO

Keywords:
CO_2-blends
Vapour-liquid equilibrium
Thermal stability
Hexafluorobenzene
Transcritical cycle
Power cycle performance

ABSTRACT

Nowadays supercritical CO_2 cycles are considered as a promising alternative to the traditional steam cycle for the power block in CSP plants with the aim of enhancing the system efficiency and reducing costs. This work deals with the experimental characterisation of a CO_2 blend as working fluid in transcritical cycle: the addition of C_6F_6 as a dopant increases the fluid critical temperature allowing for a condensing cycle in hot environment with ambient temperature higher than 40 °C. The potential benefits on adopting this mixture passes through thermal stability test for identifying its maximum operating temperature and Vapour Liquid Equilibrium measurements for tuning the Equations of State, thus having a good prediction of the thermodynamic properties. The static method with thermal stress test at different operating temperatures shows that the mixture can withstand to about 600 °C in an Inconel 625 vessel. Furthermore, the standard Peng-Robinson with the optimised binary interaction parameter is selected for a preliminary thermodynamic assessment of the power cycle. An efficiency of 41.9% is found for an optimum mixture composition with a CO_2 molar content of 84% considering a turbine inlet pressure of 250 bar and a maximum and minimum cycle temperature of 550 °C and 51 °C respectively.

1. Introduction

Concentrating solar power (CSP) plants represent one of the technology to be adopted for the decarbonization of the electricity power generation portfolio. Today they are penalised by huge capital cost that is reflected on the final Levelized Cost of Electricity (LCOE), typically in the range of 110 ÷ 270 $/MWh, that is higher than competitive renewable and fossil fuel technologies [2]. The investment costs are affected by the complexity of this solution from the solar field together with the tower and the receiver, to the thermal energy storage and the traditional steam cycle adopted as power block. Over the last years, supercritical CO_2 (sCO_2) cycles have been investigated as a promising alternative for the power block with the double aim of enhancing the CSP efficiency and reducing the costs [1]. sCO_2 cycles are characterized by extremely compact machinery and simple layouts: no bleedings, no steam drums, and a minimum operating pressure above the atmospheric pressure (higher than the CO_2 critical pressure (73.8 bar)) together with the possibility of increasing the maximum operating temperature of the power block are the main advantages of sCO_2 cycles when compared with the more traditional steam cycles [2–4]. At the current state of the art, the sCO_2 recompressed cycle can reach efficiencies up to 41.8%, at $T_{max} = 550$ °C using molten salts as heat transfer fluid (HTF) [5,6], and up to 48.9% at $T_{max} = 700$ °C with liquid sodium as innovative HTF [7,8]. Different national and European projects are working on this topic both from simulation, lab scale or pilot plant demonstration point of view. In the last years, several European projects were funded: for example, SCARABEUS [9], DESOLINATION [10], COMPASSCO2 [11], sCO2 Flex [12], sCO2-HeRo [13] or CO2OLHEAT [14]. On the other hand a proof-of-principle Brayton cycle power loop was developed at Sandia laboratory for different configuration of a pure sCO2 cycle with a maximum temperature of about 315 °C and a maximum inlet heater power of 520 kW in the recompressed cycle configuration [15] and a Supercritical CO2 Integral Experiment Loop was constructed in KAERI (Korea Atomic Energy Research Institute) [16]. Moreover small pilot plant are developed: design/control requirements were investigated for

* Corresponding author.
E-mail address: gioele.dimarcoberardino@unibs.it (G. Di Marcoberardino).

https://doi.org/10.1016/j.applthermaleng.2022.118520
Received 13 December 2021; Received in revised form 8 April 2022; Accepted 10 April 2022
Available online 13 April 2022

Nomenclature

Acronyms

BIP	Binary interaction parameter, -
CSP	Concentrated solar power
EoS	Equation of state
HP	High pressure
HTF	Heat transfer fluid
LCOE	Levelized cost of electricity, $ MWh^{-1}
LK-Plock	Lee Kesler Plocker EoS
LP	Low pressure
MITA	Minimum Internal Temperature Approach, °C
PHE	Primary heat exchanger
PR	Peng Robinson EoS
PC-SAFT	Perturbed-Chain Statistical Associating Fluid Theory EoS
REC	Recuperator
sCO_2	Supercritical CO_2 cycle
VLE	Vapour-Liquid Equilibrium

Symbols

ΔT	Temperature difference, °C
ΔP	Pressure drop, bar
h	Enthalpy, kJ/kg
$\dot{m}$	Mass flow rate, kg s^{-1}
MM	Molar mass, kgkmol^{-1}
P	Pressure, bar
Q_{th}	Thermal heat, MW
ρ	Density, kg m^{-3}
s	Entropy, kJ kg^{-1} K^{-1}
T	Temperature, °C
x_i	Species i molar fraction in liquid phase, –
y_i	Species i molar fraction in gas phase, –
W	Mechanical work, MW

Greek symbols

η_{cycle}	Cycle efficiency, –

Subscripts

c	Critical
cond	Condenser
i,j	Species
L	Liquid phase
min	Minimum
max	Maximum
pump	Pump
tur	Turbine
vap	Vapour phase

a 1 MWe-scale supercritical CO2 test loop at Southwest Research Institute simple recuperated cycle configuration at pressures and temperatures up to 255 bar and 715 °C, respectively [17]; an integrated and reconfigurable 10 MWe pilot plant was designed in STEP project [18]; or a retrofitting of the existing Shouhang's 10MWe concentrated solar power plant with a 10MWe supercritical CO2 power cycle together with EDF is discussed in [19].

In particular, the H2020 European project SCARABEUS [9] proposed an innovative solution, based on a transcritical cycle, in which the gas compression phase is replaced with a liquid compression, thus reducing the power consumption in the typical hot and arid environment for CSP applications [20] where no low temperature coolant (i.e. cold water) is available. As already suggested in previous works [7,21–23], a blend of CO_2 with a certain dopant, characterised by a higher critical temperature than pure CO_2, can result in liquid phase conditions at the inlet of the compression step for typical CSP application with a minimum cycle temperature around 50 °C while keeping the same advantages of pure CO_2 over steam Rankine cycle (e.g. the cycle compactness, a maximum operating temperature up to 700 °C).

Another important characteristic for the selection of the dopants is the working fluid thermal stability with expected values, for the highest efficiency applications, up to 700 °C. Excluding the inorganic compounds class, perfluorocarbons compounds are suggested by preliminary activities of the SCARABEUS project and other research studies [24–27]: they are characterised by good solubility into CO_2, good molecular complexity, low-toxicity and low-flammability [28] and they are potentially thermally stable and chemically inert at temperatures higher than 400 °C [25,29–32]. On the other hand, they are very expensive fluids and with a high global warming potential (i.e. 6630 for tetrafluoromethane CF_4, 11,100 for Hexafluoroethane C_2F_6 or 9550 for Octafluorocyclobutane C_4F_8 [33]).

The dopant selected in this work is the hexafluorobenzene C_6F_6, that has been already investigated in [26,34], as its aromaticity makes it the best candidate for achieving higher temperature stability [35] and it is also characterised by relatively high critical temperature and molecular complexity. The main characteristics of the two chemical species used in the experimental tests are reported in Table 1 with the link to their safety data sheets (SDS).

The procedure for the investigation of the potential of a CO_2 blend, originally described in [24], consists of three main steps: (i) the definition of the mixture thermodynamic properties and behaviour at different pressures and temperatures including the two-phase region with a reliable Equation of State (EoS) calibrated on Vapour-Liquid equilibrium data, (ii) the thermal stability to identify the maximum operating temperature of the mixture and (iii) the preliminary design and performance evaluation of the power plant adopting the innovative mixture as working fluid. As a matter of fact, there are no thermal stability data available in the literature for the investigated dopant and the CO_2 blend but just few experimental thermal stability test with both static and dynamic systems revealed that a mixture of

Table 1
Characteristics of the fluids.

Name	CAS number	MW (kg/kmol)	T_{cr} (°C)	p_{cr} (bar)	Expected Thermal stability (°C)	Supplier	Purity level (% mol)	SDS
CO_2	124–38-9	44.01	31.06	73.83	> 700	Rivoira S.p.a. (VLE)	99.998	https://nippongases.com/api/search/getExternalFile/4774519/Anidride%20carbonica%20CO2%20Safety%20Data%20Sheet%20SDS%20018ARGpdf
						Sol S.p.a. (Th. Stability)	99.99	http://www2.sol.it/msds2/MS018A_MS_1_1_3.pdf
C_6F_6	392–56-3	186.06	243.58	32.73	> 480 [29]	Alfa Aesar (ThermoFisher GmbH)	>99	https://www.alfa.com/it/msds/?language=EE&subformat=CLP1&sku=A11500

pentafluorobenzene C_6HF_5 and hexafluorobenzene (with a composition of 60% and 40 % molar fraction respectively) can work at around 480 °C [29]. Whilst, regarding the binary mixture $CO_2 + C_6F_6$, only one data set of experimental bubble points for seven isothermal vapour-liquid equilibrium (VLE) conditions (from 20 to 80 °C) are available in literature for the calibration of thermodynamic properties [36].

In this work, the procedure, described above, is applied to the mixture $CO_2 + C_6F_6$ from both experimental and modelling point of view. New VLE experimental data were carried out at LEAP Laboratory [37] within the SCARABEUS project together with mixture thermal stability tests, performed at Fluids test lab of University of Brescia [38] to cover the lack of the information on the investigated mixture. The experimental activities are required (i) to calibrate and optimise the thermodynamic property models for the prediction of the real mixture behaviour and (ii) to set the maximum operating temperature of the mixture for the cycle design. These outcomes thus contribute to a complete and reliable analysis of the $CO_2 + C_6F_6$ transcritical cycle. The paper consists of three main sections: the first is devoted to the discussion of the VLE data measurements and the choice of the proper optimised property model for the prediction of the mixture behaviour; Section 3 covers the thermal stability methodology and its results using two different materials for the sample cylinder; cycle modelling and system performance are then investigated in Section 4.

2. CO_2 based mixture behaviour

2.1. Vapour-liquid equilibrium test

The vapor-liquid equilibrium measurements (P,T,x,y) have been carried out by using the experimental apparatus designed and manufactured in 2012 by ARMINES and installed at LEAP laboratory, already described in [39,40]: it is based on a static-analytical method [41] and, originally, it was conceived to measure equilibrium properties of CO_2 based mixtures relevant for oxy-combustion Carbon Capture and Storage (CCS) strategy [42].

Prior to the VLE analysis on CO_2, the calibration of the main instruments, such as pressure transducers, temperature probes and gas chromatograph (GC), has been performed. As a result, the four temperature sensors are characterised by an estimated expanded measurement uncertainty (with a coverage factor k = 2) of 0.08 K in a temperature range of 213–473 K while the three pressure transducers, with a full-scale respectively of 2 MPa, 6 MPa and 20 MPa has showed an estimated expanded measurement uncertainty (with a coverage factor k = 2) of 0.005 MPa.

The procedure for the GC calibration is here described. First, the chemical species are introduced in the GC columns using a very small volume manual syringes in order to withdraw a sample of the substance (from the vessel in case of C_6F_6 and from the cylinder in case of CO_2). Then, the thermal conductivity detector (TCD) of a GC produces as output an electrical signal (measured in μV) proportional to the rate of the substances which are flowing through it. The chromatogram (or chromatographic diagram) is the combination of this information with the retention time (i.e. the time span for a specific substance to completely pass through the chromatographic column). Fig. 1 shows an example for a binary mixture of CO_2 and C_6F_6. In the chromatographic diagram, the area A_i subtended by each chromatogram peak (measured in units μVs), is proportional to the amount of the specific substance n_i passed through the TCD. Once this relationship is known, it is then possible to determine the molar fraction z_i of each component of a mixture, and the uncertainty u_{n_i} associated to the measurement of each z_i.

The combined uncertainty u_{n_i} of each GC calibration point, relative to the number of injected moles $n_{inj,i}$ with the syringe, can be calculated with the error propagation theory taking into account the different uncertainty sources associated to each composition measurement, and so to the amount of moles n_i of each species of the mixture. One source of error is related to the uncertainty of the estimated number of moles of each component introduced through syringes from the injected volumes of each fluid and considered as calibration reference: this is a function of the syringe volume, temperature and pressure of the fluids inside the syringes. For this purpose, the reference density of the carbon dioxide is calculated by the Span and Wagner EoS implemented in REFPROP [43] $\widetilde{\rho}_{ref_i}(T_{amb},P_{amb})$, whereas for the hexafluorobenzene has been taken from [44]. The other one is the standard deviation associated to the mean measured area. A detailed and comprehensive description and calculation of the uncertainty associated to the GC measurements can be found in a previous work [45]. The left side of Fig. 2 shows the total uncertainty for the CO_2 calibration function as long as the single contributions, revealing that the major source of uncertainty is related to the accuracy of the syringes. Fig. 3 shows the results for the calibration function of C_6F_6. Looking at the right side of both Fig. 2 and Fig. 3, it is worth noting that the mean values of the residuals (calculated as the difference between number of moles injected and estimated by GC) are included in the confidence region, delimited by the two lines that interpolate the punctual relative uncertainties of the injected number of moles (Figure left side).

A calibration model is so obtained for the evaluation of the mole fraction and the relative expanded uncertainty from a chromatogram measurement for both the chemical species. The generic expression to fully characterize a composition measure is described below while Table 2 reports the resulting parameters of the GC calibration for both CO_2 and C_6F_6.

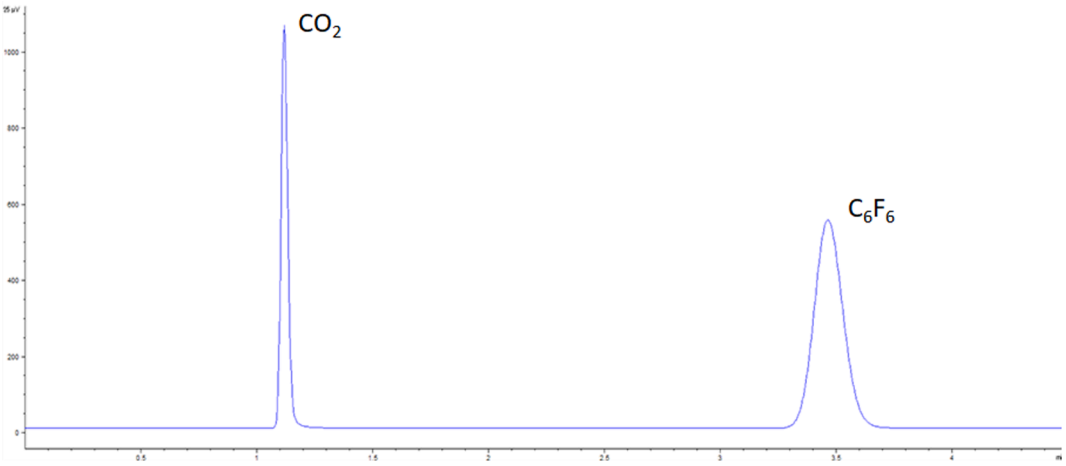

Fig. 1. Output of the TCD for a mixture of CO_2 (peak in the left) and C_6F_6 (peak on the right).

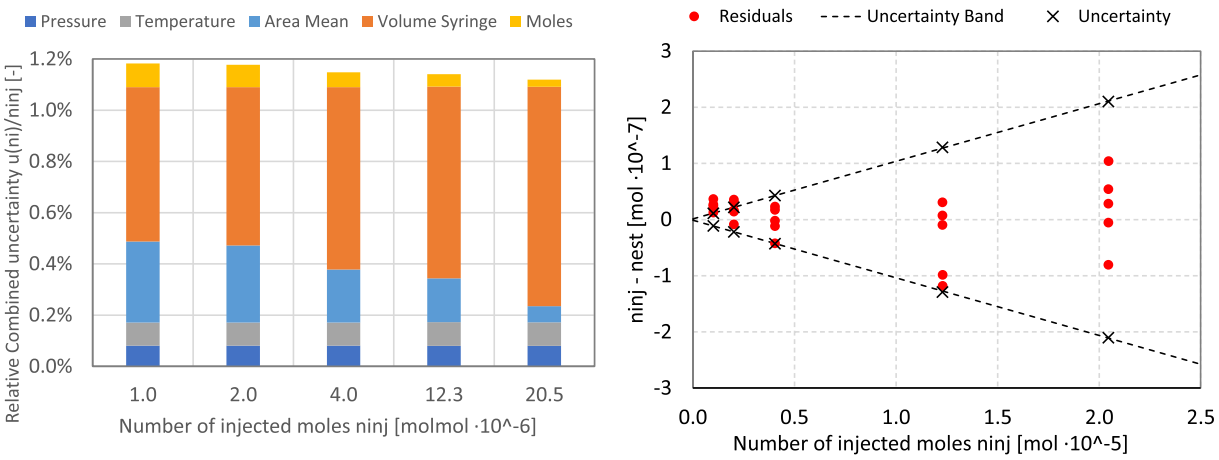

Fig. 2. Uncertainty sources (left) and residuals with uncertainty bands (right) in case of CO_2.

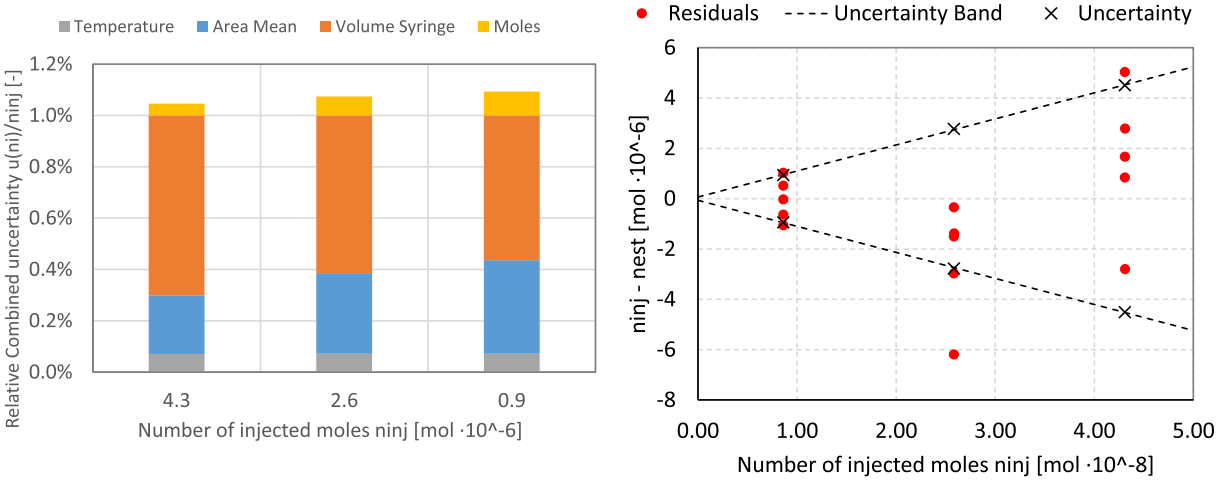

Fig. 3. Uncertainty sources (left) and residuals with uncertainty bands (right) in case of C_6F_6.

$$\begin{cases} \tilde{n}_j(A_j) = \bar{a}_j A_j \\ \tilde{u}_{n_j}(n_j) = \bar{b}_j n_j + \bar{c}_j \end{cases} \quad (1)$$

In this experimental campaign new VLE data for the investigated mixture has been collected at 3 isotherms (323.15 K, 343.25 K and 363.08 K) with pressure values ranging from 1.0 MPa to 11.4 MPa. All the apparatus parameters, as shown in Table 3, are set and kept constant according to the values adopted for the experimental campaign. Finally, the temperature of the thermostatic bath is set to the desired value of the isotherm under measurement, waiting until stabilization, with the cell immersed in the bath.

The resulting binary diagrams and equilibrium ratio (Ki) diagrams (vapor composition to liquid composition) are depicted in Fig. 4. The collected experimental data are shown in Table A.1. Due to the long waiting time in reaching the equilibrium of the liquid phase at low pressure and temperature, basically caused by a slow diffusion of the CO_2 in the liquid C_6F_6 in the equilibrium cell, the binary VLE diagram at 323.15 K is partially defined.

Table 2
Results of the gas chromatograph calibration.

Substance	$\bar{a}_i$[mol/μVs]	$\bar{b}_j$[−]	$\bar{c}_j$[mol]
CO_2	$1.873 \cdot 10^{-10}$	0.01026	$1.2753 \cdot 10^{-9}$
C_6F_6	$7.908 \cdot 10^{-11}$	0.01035	$6.7937 \cdot 10^{-10}$

2.2. Equation of state characterisation

Two sets of experimental VLE data are available for the mixture CO_2 + C_6F_6: the one discussed in the section above from Leap and the other one from the literature (Dias et al. [36]). The first set presents both bubble and dew points at three isothermals (50 °C, 70 °C and 90 °C) but the data at 50 °C are discarded as they cover few mixture compositions at two different pressure range; on the other hand, the second accounts for only bubble points at different isothermals from 20 to 80 °C.

In a binary mixture, the mutual interaction between the two fluids is particularly evident in the two-phase region where the partial molar properties and the partial derivatives of the variables computed for the mixture are a function of the mixture composition in the gas and liquid phase. For this reason, the VLE experimental data can be used to empirically calibrate the binary interaction parameter (BIP) of a predictive EoS in order to properly compute the real behaviour of the

Table 3
Values of the main set parameters during the experimental campaign.

Main Experimental Apparatus Parameters	Value
GC oven temperature	413 K
TCD temperature	473 K
Transfer line (between ROLSI™ samplers and GC column) temperature	343 K
PTs heated support temperature	358 K
Vapour and liquid phase sampling time	0.25 s
GC maximum analysis time	5 min

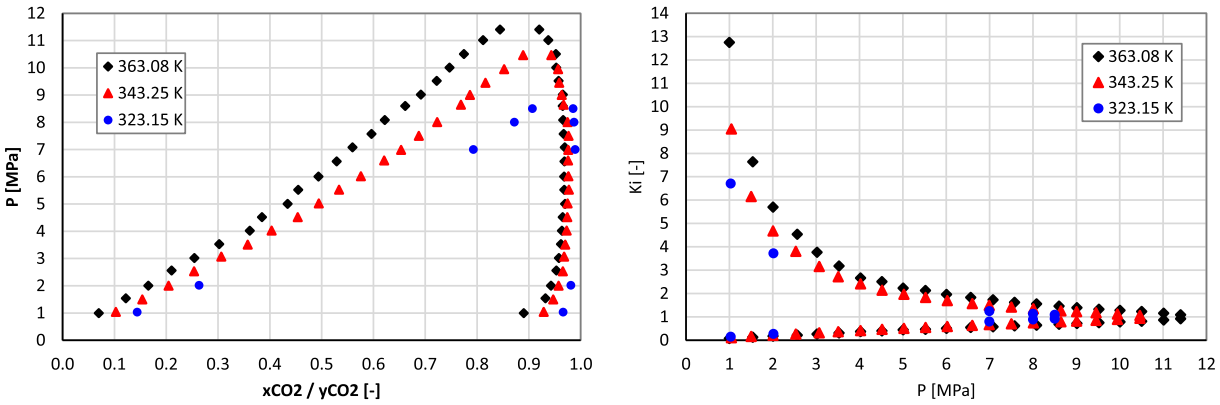

Fig. 4. Experimental VLE data for the binary mixture of CO_2 and C_6F_6 (left). Equilibrium ratios (right): the upper curves are for CO_2 while the lower ones are for C_6F_6.

Table 4
Binary interaction parameters for the investigated EoS.

	Standard PR EoS	LK-Plock EoS	PC-SAFT EoS
k_{ij}	$0.16297 - 0.0003951 \cdot T\,[K]$	0.085	$0.1023 - 0.05574/(T/298.15\,[K])$

mixture.

In this work, three property models, that are already applied to supercritical CO_2 cycles, are considered: the well-known cubic Peng Robinson EoS (PR) with the simple van der Waals mixing rules [35], a virial model LK-PLOCK [47,48] and an Helmholtz free energy equations the PC-SAFT [49]. In the cubic equations and virial equations, the solution of the equation is an explicit formulation of $v = f(T,P)$, or, in case of mixtures, $v_{mix} = f(T,P,x_i)$. On the other hand, in a Helmholtz free energy explicit equation, the solution of the equation is a formulation $a = f(T,P)$, or $a_{mix} = f(T,P,x_i)$ for mixtures, where a is the Helmholtz free energy of the modelled fluid. The main pure component parameters, that are required by the different EoS for the definition of the mixture behaviour, are reported in [26].

As a matter of fact, the accurate calibration of the EoS in the VLE region and its phase composition is widely accepted in scientific literature as the best way to approach, at least at the first stage, the optimization of the EoS. Considering the classic mixing rules of cubic EoS, for examples, the BIP usually plays a significant role in computing partial derivatives, the quantities that most influence the fugacity coefficients and hence the VLE calculations. Furthermore, looking at the shape of the VLE curve, as can be noticed in Fig. 4, the bubble point are the most important ones in fitting the BIP, since they cover the wider range of compositions and therefore they are the most sensitive parameter to pressure variations.

The EoS calibration is carried out with the software ASPEN Properties v11 [46] by fitting the respective BIP on the experimental VLE data. The maximum likelihood method is adopted as numerical optimization method, in order to fit both the bubble pressure and the dew composition, when the bubble and dew compositions are given as input. The resulting mean absolute percentage error (MAPE) is chosen as the index for the EoS accuracy in fitting the VLE properties: it is computed for both the bubble pressures and the molar compositions at dew conditions using the formula below. The BIP parameters determined by the VLE data regression are shown in Table 4. For each property model, both constant values and expressions of BIP = f(T) are considered: the one with the low standard deviation is chosen for the MAPE comparison.

$$MAPE_X = \frac{1}{N}\cdot\sum_{i=1}^{n}\left|\frac{X_{\text{Actual}} - X_{\text{Estimated}}}{X_{\text{Actual}}}\right| \quad (2)$$

Table 5 and Table 6 show the MAPE on VLE calculation for the three investigated EoS: the first table covers the overall pressure range for the

Table 5
Median Average Percentage Error (MAPE) for the CO_2 + C_6F_6 mixture VLE experimental data, computed with various EoS.

	MAPE: P bubble Dias					
	40 °C	50 °C	60 °C	70 °C	80 °C	Average
PR	2.4%	2.2%	2.1%	2.3%	2.8%	2.4%
LK-PLOCK	3.2%	3.3%	2.5%	1.8%	1.7%	2.6%
PC-SAFT	7.0%	6.4%	5.4%	4.5%	3.7%	5.4%

	MAPE: Leap Experimental data					
	P bubble			Y dew		
	70°C	90°C	Average	70°C	90°C	Average
PR	2.1%	3.6%	2.8%	0.5%	2.6%	1.6%
LK-PLOCK	2.5%	5.9%	4.2%	0.3%	1.7%	1.0%
PC-SAFT	5.3%	7.9%	6.6%	0.4%	2.1%	1.2%

Table 6
Median Average Percentage Error (MAPE) for the CO_2 + C_6F_6 mixture VLE experimental data, computed with various EoS, only when the relevant pressures (P > 30 bar) are included in calculations.

	MAPE: P bubble Dias (P > 30 bar)					
	40 °C	50 °C	60 °C	70 °C	80 °C	Average
PR	2.0%	1.4%	1.2%	1.7%	2.4%	1.7%
LK-PLOCK	3.2%	3.7%	2.4%	1.7%	1.3%	2.5%
PC-SAFT	2.5%	2.8%	2.6%	2.2%	2.3%	2.5%

	MAPE: Leap Experimental data (P>30 bar)					
	P bubble			Y dew		
	70°C	90°C	Average	70°C	90°C	Average
PR	2.3%	3.0%	2.6%	0.5%	2.0%	1.3%
LK-PLOCK	2.0%	6.4%	4.2%	0.3%	1.2%	0.7%
PC-SAFT	4.7%	7.9%	6.3%	0.3%	1.5%	0.9%

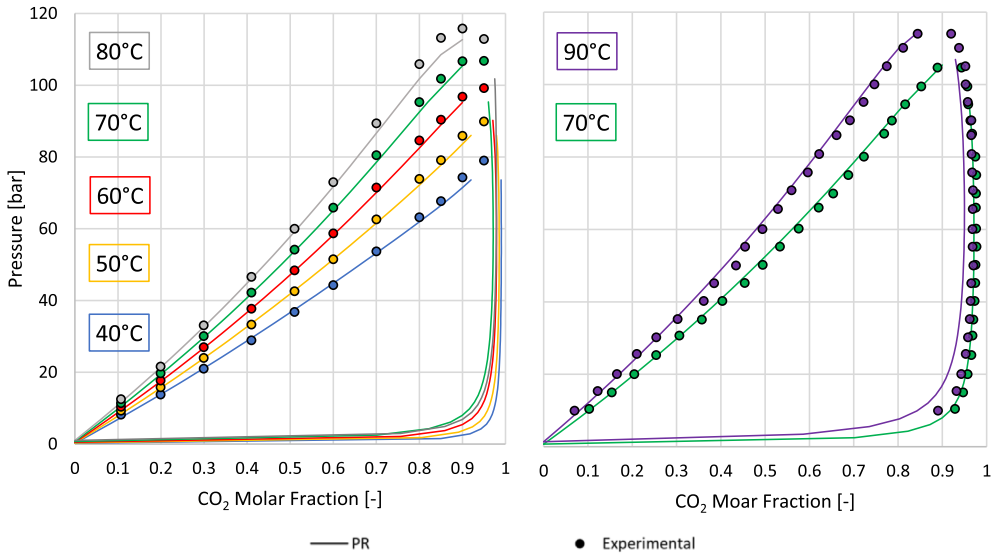

Fig. 5. Graphical fitting of the experimental VLE data for the $CO_2 + C_6F_6$ mixture with the standard PR EoS and its optimized BIP. Experimental data from Dias et al. (left), Leap laboratory (right).

isothermal lines from 50 to 90 °C, the second one refers to VLE data with pressures higher than 30 bar. The latter is used for the choice of the more reliable EoS because (i) the minimum operating pressure of the power cycle simulation will be higher than the considered pressure limit, (ii) at low pressure, the relative error becomes two-three times higher than MAPE values at higher temperature.

The best fitting EoS turns out to be the standard Peng Robinson EoS, with temperature dependent BIP: the selected equation can fit both the experimental dataset with lower average MAPE values for all the data excluding the dew composition for the Leap isothermal lines. A qualitative comparison between the simulated VLE with the corresponding best fitting EoS (solid lines) and the experimental data (dots) is presented in Fig. 5.

Once the property model is defined, the main mixture thermodynamic properties, saturation lines and phase behaviour in low temperature region can be represented through pressure–temperature (p-T), temperature-entropy (T-s) or density-temperature (ρ-T) charts for specific mixture compositions. The characterisation of the mixture with a CO_2 content of 80% is shown in Fig. 6. In the three graphs, the critical point of the mixture (125 °C and 123 bar) is highlighted with a black diamond: this composition is suitable for SCARABEUS application as the critical point temperature is relatively higher than the minimum cycle temperature (about 50 °C). In T-s and ρ-T diagrams, some isobaric lines of interest for the SCARABEUS transcritical cycle are depicted: in particular, isobars from 60 to 80 bar are reported because they have bubble temperature in the range 40–60 °C, typical for condensation. From the p-T diagram (Fig. 6 top), it can be seen that the temperature glide (temperature difference between bubble and dew point at a given pressure) is significant: for example, for a bubble pressure (at 50 °C) of 74 bar, it is about 100 °C. This aspect is important for the design of the components in the low-pressure side of the cycle (the hot-side of the recuperator and the condenser). In the T-s diagram (Fig. 6 left-bottom), the temperature difference across the pump (at least for an isentropic process) can be quantified together with the other thermodynamic transformations that occur in a transcritical cycle (i.e. heat introduction, turbine expansion). Finally, the ρ-T diagram (Fig. 6 right-bottom) can be useful for the evaluation of the compressibility effects in the pump region: in particular, it gives a qualitative idea of the isothermal compressibility factor β_T ($\beta_T \propto \left(\frac{\partial v}{\partial P}\right)_T$) which differs from mixtures to mixtures and depends on composition.

3. CO2 based mixture: thermal stability

The thermal stability of a pure fluid or a mixture represents its "heat resistance", or the capability to preserve unchanged all its main thermophysical properties following heating [47]. This is a key parameter for the selection of a working fluid in a power plant as a partial decomposition may decrease the cycle performance and/or cause technical issues in the main power block components, such as heat exchangers and fluid machines. So the thermal stability analysis aims at the evaluation of the maximum operating temperature range of the working fluid that can adopted in a power cycle.

The methodology assessed for the thermal stability tests in the SCARABEUS project is summarised Fig. 7. A static method, where the fluid (or the mixture) is confined in a vessel in steady-state condition, is considered in this work. The thermal stability is assessed through experimental tests where the sample is heated up in steady-state conditions at different operating temperatures for a limited period of time. The fluid degradation is then assessed by comparing the behaviour of the fluids along curves at constant specific volume (isochoric lines) before and after each thermal stress tests at high temperature, measuring two main thermodynamic properties, pressure and temperature. The deviations of the isochoric line with respect to the reference obtained from the fresh fluid, caused by the thermal decomposition, are evaluated both at high temperatures, during the thermal stress tests, and at temperature close to ambient conditions. This qualitative method can be sufficient for the identification of possible fluid thermal degradation process.

The test circuit for the SCARABUES project, shown in Fig. 8, consists of one sample cylinder (A), 4 needle valves (B), 2 pressure transmitter (C), one fitting (D) for the connection with the fluid or helium bottles or with the vacuum pump and 1 thermocouple (not shown in the figure) that is put in contact with the sample cylinder externally. The needle valves position (on/off) allows to: (i) loading the sample and close the circuit during the tests (valve B4), (ii) using or not the pressure transmitter C1 (valve B2) with a maximum full scale of 10 bar, (iii) using or not the pressure transmitter C2 (valve B3) with a maximum full scale of 60 bar, (iv) disconnecting the sample cylinder (valve B1) with the investigated sample at the end of the test. The test circuit is enveloped by the electric heaters (and thermally insulated with mineral wool) as represented with a dashed red line in Fig. 3. The main components of the test circuit and the instruments are listed in Table 7 and Table 8 respectively. Preliminary tests on pure CO_2 and the blend CO_2-C6F6 were carried out with sample cylinder in stainless steel while a custom

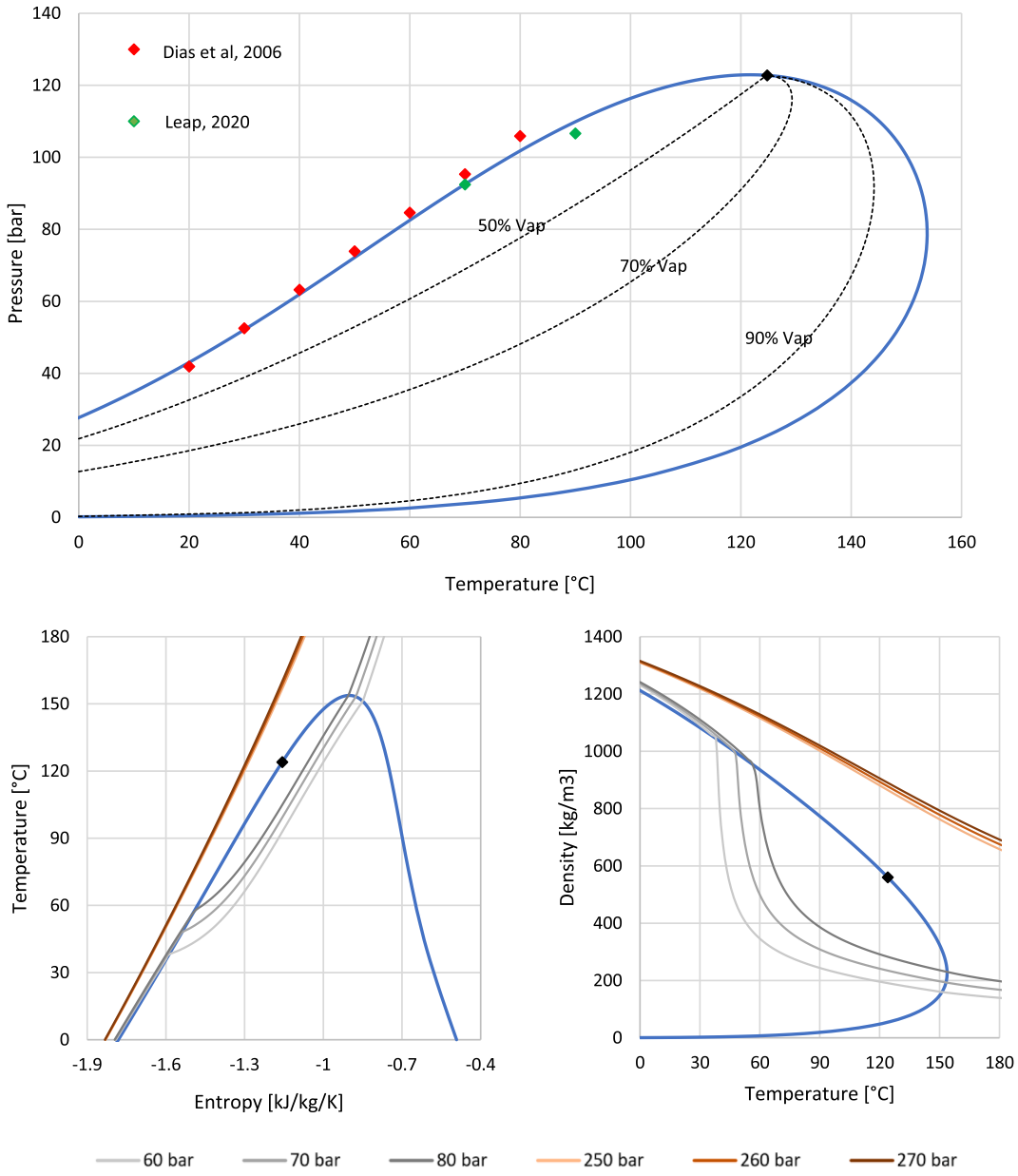

Fig. 6. P-T, T-s and ρ-T plots representing the thermodynamic and volumetric behaviour of the mixture CO_2 + C_6F_6 with the standard Peng Robinson EoS and optimized BIP, when z_{CO_2} = 80% molar fraction is selected.

model designed and manufactured by Officine Orsi [48] in Inconel 625 was used for all the ultimate thermal stability stress test. Additional details on the experimental apparatus are discussed in [49]. The test circuit was not designed to control the pressure during the thermal stability, so the operating pressure is a consequence of the amount of fluid loaded in each test and of the operating temperature of the thermal stability stress test. Thus, for all the tests, the mass of the sample fluid is defined on the requirement of keeping the system pressure below a safety value of 60 bar; while the investigated composition of the mixture is chosen in the range of interest for SCARABEUS project [23,26].

Two thermal stability tests for a fresh mixture of CO_2 + C_6F_6 with a CO_2 content of 80% are carried out by adopting two sample cylinders made with different materials: first a sample cylinder in stainless steel AISI 316L (internal volume of 150 cm^3) was used, then the test was performed with a sample cylinder in Inconel 625 (internal volume of 220 cm^3). The same test procedure is applied in both the rounds but, considering the difference in the vessel material and internal volume, the investigated thermal stress temperature and the amount of fluid loaded in the test circuit were different. After a preliminary leakage test of the test circuit with helium, the air and other possible pollutants inside the test circuit were removed thanks to a vacuum pump reaching absolute pressure of 1–10 mbar. So the test circuit weight was measured by an electronic scale at sub-atmospheric condition: the measured mass value can be then used for the estimation of the mass of the sample loaded. The dopant was charged first in the sample cylinder, at sub-atmospheric pressure, thanks to a calibrated syringe. Then the test circuit was placed in the thermostatic bath at 0 °C and connected to the CO_2 bottle for loading. The test circuit weight was measured before and after each loading phase in order to estimate the mass of the sample loaded, as reported in Table 9. The fresh mixture density, equal to 45 kg/m^3, is determined by the ratio of the weighted mass loaded in the circuit and the internal volume of the sample cylinder. The experimental procedure starts with the analysis of the mixture behaviour at different operating temperature defining the reference isochoric line. After that, different thermal stress tests at steady-state conditions are carried out in an electric oven at high temperatures, followed by the measure of the

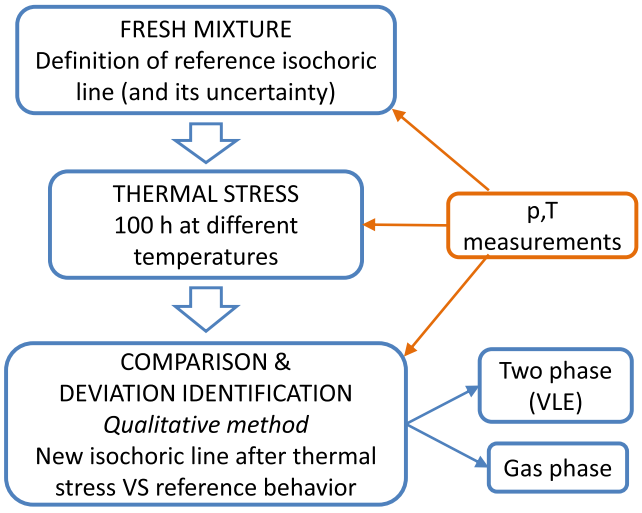

Fig. 7. Thermal stability test methodology.

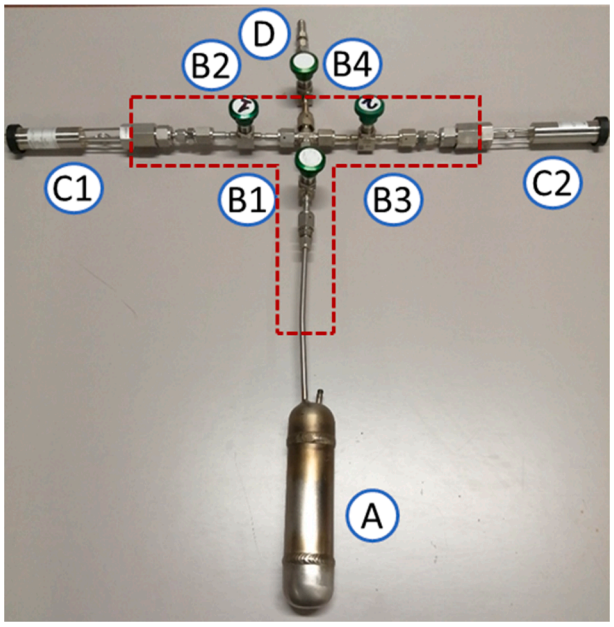

Fig. 8. SCARABEUS test circuit.

Table 7
Test circuit equipment.

Type	Brand	Model	Characteristics
Sample cylinder	Swagelok	316L-50DF4-150	Internal Volume 150 cm^3 Material SS316L
Sample cylinder	Officine Orsi	Custom model manufactured for SCARABEUS	Internal Volume 220 cm^3 Material Inconel 625
Needle valves	Swagelok	SS-4H-V13	–
Electric heaters	Isopad	S45 2 M	500 W (230 Vac)
Vacuum pump	DamiCosmos	MP90DEVV	P min 1 mbar
Scale	Mettler-Toledo	MS12002TS	FS: 12.2 kg – Accuracy 0.1 g

Table 8
Test circuit instruments.

Type	Acronym	Brand	Model	Measurement range	Accuracy
Pressure transmitter	C1	Keller	PA – 35X HTC	0.0.10 bar	0.5 % of full-scale
Pressure transmitter	C2	Keller	PA – 35X HTC	0.0.60 bar	0.5 % of full-scale
Thermocouple	–	Tersid	Type K	−200.0.1270 °C	1.5 °C

Table 9
CO_2 + C_6F_6: Fluid loading weight measurements.

Fluid charge	First round (SS 316L) Weight (g)	Second round (Inconel 625) Weight (g)
Test circuit (empty)	2506.3	3151.7
Test circuit (with C_6F_6)	2510.3	3157.4
Test circuit (with mixture)	2514.0	3162.8
Total Sample fluid	7.7	11.1
CO_2	3.7	5.4
C_6F_6	4.0	5.7

Table 10
CO_2 + C_6F_6: Thermal stability test conditions.

Isochoric line			Thermal stress		
T (°C)	ΔT_{step} (°C)	$Time_{step}$ (min)	T (°C)	ΔT_{step} (°C)	$Time_{step}$ (h)
20 ÷ 250	20 for T ≤ 120 10 for T > 120	15	300 ÷ 550 (1st round) 400 ÷ 650 (2nd round)	50	100

isochoric line. In particular, the experimental test conditions of the investigated mixture are summarized in Table 10. Regarding the isochoric line, measurements of pressure and temperature are recorded every 1 s at equilibrium conditions with a time step of 15 min at each investigated temperatures. The data acquisition frequency moves to 5 s reporting an average value every 30 min (thus 180 recorded samples) during the 100 h foreseen for each thermal stress temperature. At the end of each activity, no change on test circuit weight was detected.

Concerning the first round, the average values of temperature and pressure obtained from the isochoric line test of the fresh fluid are reported in Table A.1 while, as an example, Fig. 9 shows experimental values recorded at 20 °C and 170 °C respectively. The uncertainty estimation takes into account both the systematic error due to the instrument accuracy (Type B standard uncertainty) and the statistical error due to the experimental standard deviation of the mean value (Type A standard uncertainty).

Regarding the thermal stress tests, Fig. 10 shows, for example, the experimental data collected at 450 °C. As both the pressure and temperature deviation are under 1% with respect to the starting point assumed as reference, there are no evidence of thermal degradation phenomena during the 100 h.

Finally, Fig. 11(top) presents the isochoric line measured after each thermal stress test with respect to the reference curve. The qualitative comparison method allows the identification of potential decomposition phenomena if the deviation of one or more (p,T) points after each thermal stress test (including its uncertainty) stands outside the reference isochoric limits that are calculated by fitting the experimental data with both uncertainties in × data and y data (black dotted lines in Fig. 11 (bottom)). For this purpose, the absolute pressure difference of the

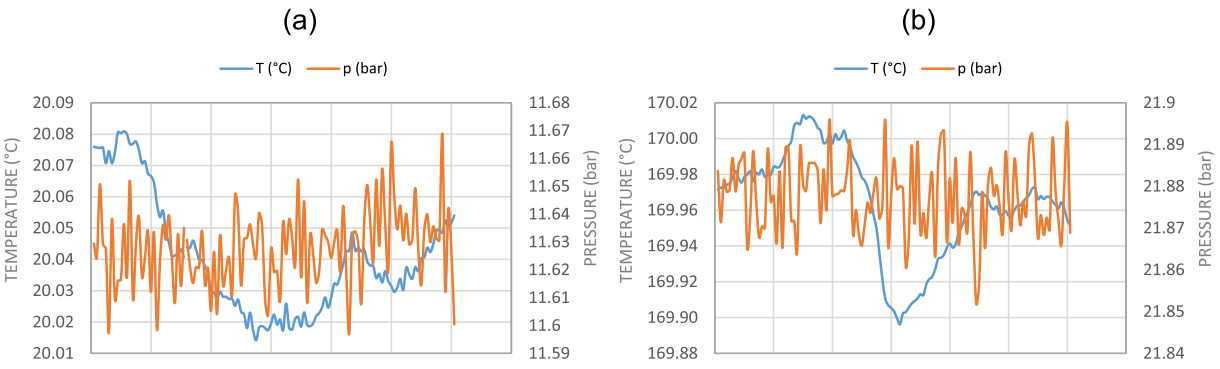

Fig. 9. $CO_2 + C_6F_6$ 1st round: Example of experimental T and p recorded in the 15 min time step: (a) T = 20 °C, (b) T = 170 °C.

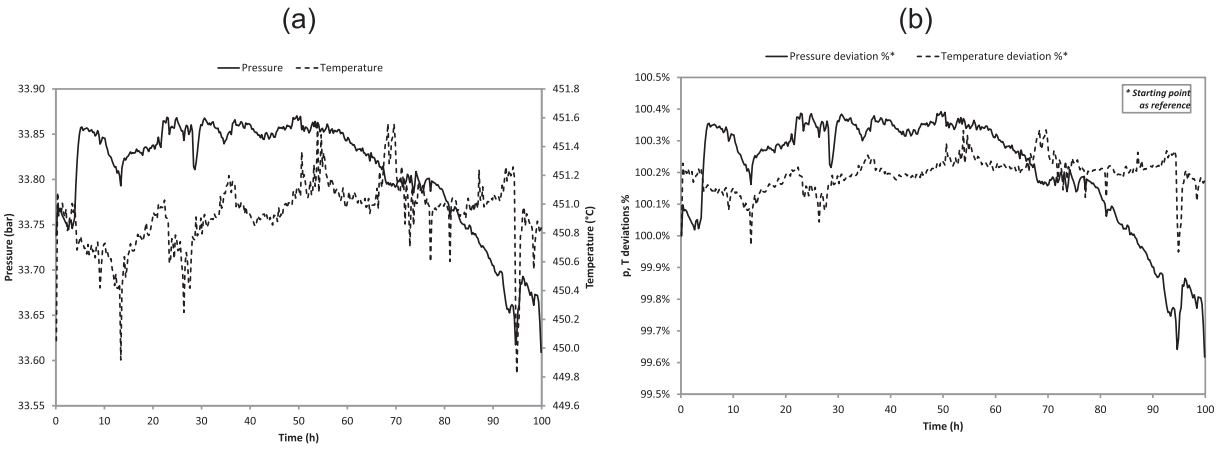

Fig. 10. $CO_2 + C_6F_6$ 1st round: (a) Experimental p and T measurements during thermal stress test at 450 °C, (b) Deviation of p and T measurements during thermal stress test at 450 °C with respect to the starting point assumed as reference.

isochoric lines with respect to the reference are depicted in Fig. 11 (bottom). The region around the dew line (temperature range of 100–160 °C) is not considered in this analysis as the mixture behaviour is influenced by the phase transition. Although no significant deviations can be found in the two-phase region, a focus on the gas behaviour, for temperature higher than 160 °C, shows significant pressure deviations for all the temperatures after thermal stress test at 500 °C. So the analysis suggests that the mixture $CO_2 + C_6F_6$ in a sample cylinder made with SS316L can be considered thermally stable below 500 °C. This test confirms some preliminary results discussed in a previous work [24] about the thermal stability of pure CO_2 in a steel vessel.

Concerning the second round, the average values of temperature and pressure obtained from the isochoric line test of the fresh fluid are reported in Table A.3 while, as an example, Fig. 12 shows experimental value recorded at 40 °C and 150 °C respectively. Regarding the thermal stress tests, Fig. 13 shows, for example, the experimental data collected at 500 °C.

As already discussed in the results of the first round above, Fig. 14 (top) presents the isochoric line measured after each thermal stress test with respect to the reference curve while Fig. 14 (bottom) shows the absolute pressure difference of the isochoric lines with respect to the reference isochoric limits that are calculated by fitting the experimental data with both uncertainties in × data and y data. Two zones are not considered in this analysis: the first one, around the dew line (temperature range of 100–160 °C), due to the mixture behaviour is influenced by the phase transition; while the experimental measurements carried out in the thermostatic bath at temperature between 150 and 190 °C are not consistent, as can be seen in Fig. 14 (bottom), because of the malfunctioning of the thermostatic bath at high temperature. The test circuit is then placed in the electric oven for the last (p,T) points of the isochoric lines at temperature higher than 200 °C. It should be also noticed that the reference isochoric values from 200 to 250 °C are linearly extrapolated from the previous data in the same gas-phase region.

After thermal stress test at 650 °C, the overall mixture behaviour changed drastically while, looking at the two-phase region (from 20 to 100 °C), the experimental data after the thermal stress test at 600 °C are quite far from the reference pressure, but still remain in the confidence region (one exception can be found at 100 °C). In this last case, a chemical analysis could be useful to have a full picture of the decomposition phenomenon, checking the extent of possible small signs of thermal degradation. As a final remark, the analysis suggests that the mixture $CO_2 + C_6F_6$ with a sample cylinder made in Inconel 625 can be considered thermally stable up to 600 °C.

Additional 300 h long-term thermal stress test was performed with the investigated mixture using Inconel 625 as sample cylinder material at 500 °C and 550 °C. The aim of this experimental campaign is to confirm the mixture behaviour in a long time period at the maximum operating temperature set in the next section for the thermodynamic analysis. In this case, the qualitative comparison of the isochoric line measure before and after the thermal stress test is focused only in the two-phase region, where, as discussed in the paragraph above, possible pressure deviations are more evident. Table 11 summarises the characteristics of the long-term test. A fresh mixture of $CO_2 + C_6F_6$ with a CO_2 content of 80% for the thermal stress test at 500 °C and 92% for the thermal stress test at 550 °C respectively is loaded in two different sample cylinders. The test procedure is similar to the one described above but the and the amount of fluid loaded in the test circuit were different.

Fig. 15 presents the isochoric line measured after the thermal stress test at 500 °C (top) at different time period (50, 100 and 300 h) and after

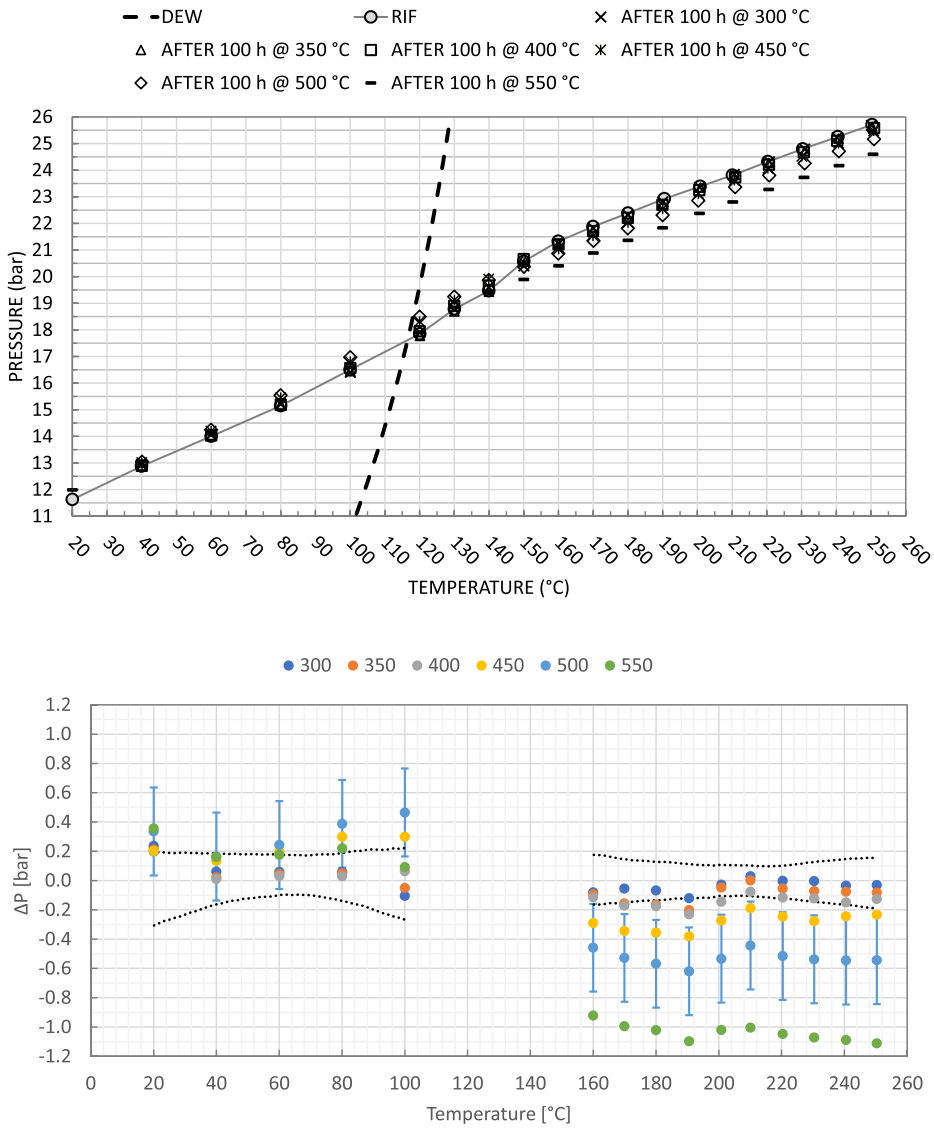

Fig. 11. $CO_2 + C_6F_6$ 1st round: Isochoric behaviour reference & after each thermal stress test (top) – Pressure difference between the isochoric behaviour reference & measurements after each thermal stress test (bottom). The black dotted lines represent the uncertainty of the isochoric reference.

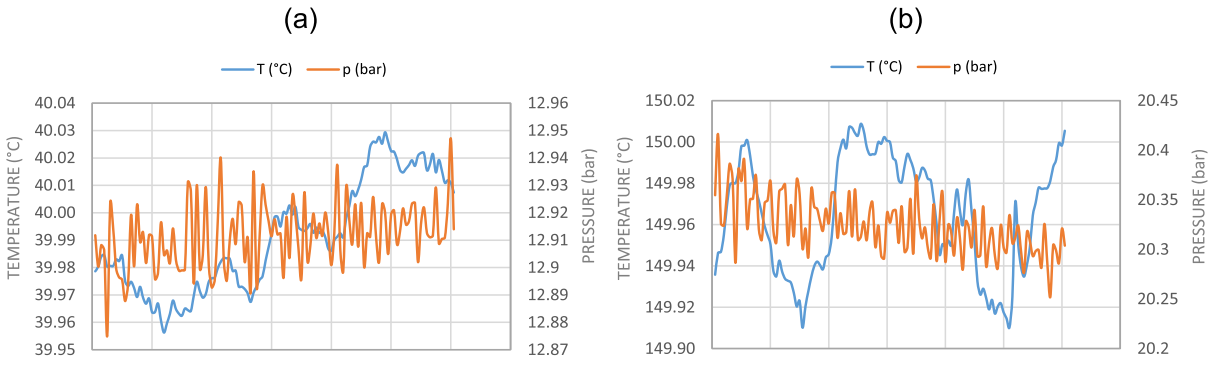

Fig. 12. $CO_2 + C_6F_6$ 2nd round: Example of experimental T and p recorded in the 15 min time step: (a) T = 40 °C, (b) T = 150 °C.

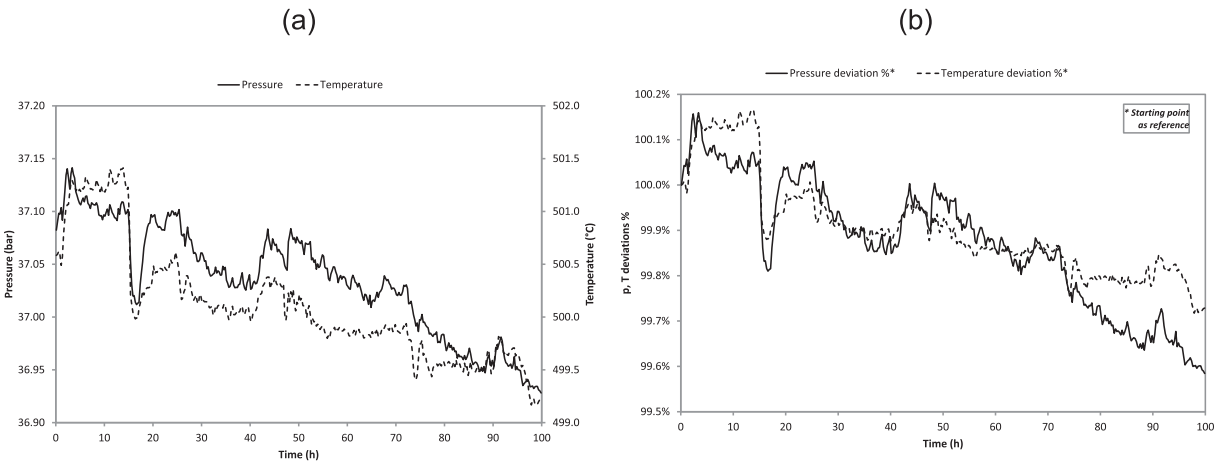

Fig. 13. $CO_2 + C_6F_6$ 2nd round: (a) Experimental p and T measurements during thermal stress test at 450 °C, (b) $CO_2 + C_6F_6$ 2nd round: Deviation of p and T measurements during thermal stress test at 500 °C with respect to the starting point assumed as reference.

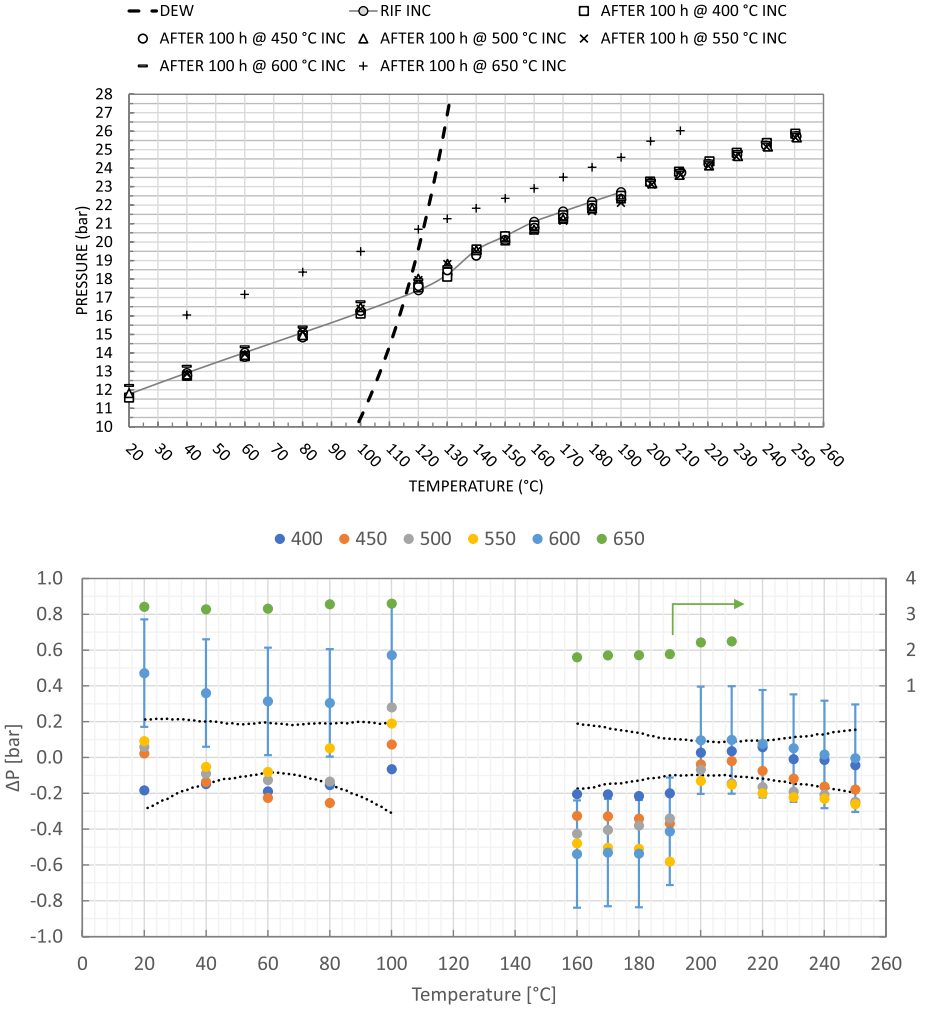

Fig. 14. $CO_2 + C_6F_6$ 2nd round: Isochoric behaviour reference & after each thermal stress test (top) – Pressure difference between the isochoric behaviour reference & measurements after each thermal stress test (bottom). The black dotted lines represent the uncertainty of the isochoric reference.

Table 11
$CO_2 + C_6F_6$ 300 h long-term test: fluid loading weight measurements and test conditions.

	300 h at 500 °C (Inconel 625)	300 h at 550 °C (Inconel 625)
Fluid charge (weight in g)		
Test circuit (empty)	2506.81	24712.12
Test circuit (with C_6F_6)	2512.44	24714.50
Test circuit (with mixture)	2517.78	2482.95
Total Sample fluid	10.97	8.83
CO_2	5.34	6.45
C_6F_6	5.63	2.38
Isochoric line		
T (°C)	20 ÷ 100	−30 ÷ 70
ΔT_{step} (°C)	20	20
$Time_{step}$ (min)	15	15

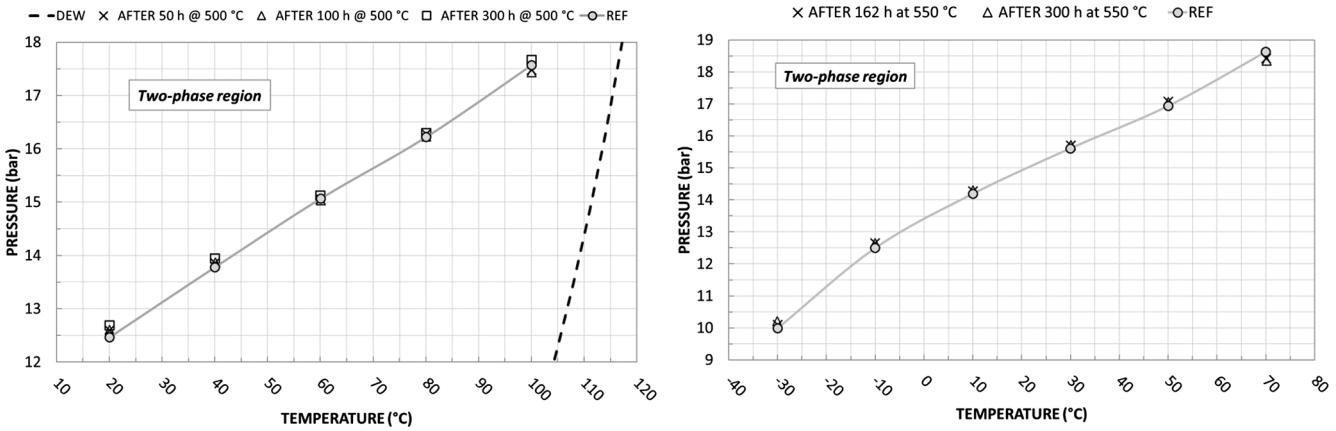

Fig. 15. $CO_2 + C_6F_6$ 300 h long-term test: Isochoric behaviour reference & after thermal stress test at 500 °C (top) – Isochoric behaviour reference & after thermal stress test at 550 °C (bottom).

the thermal stress test at 550 °C (bottom) at different time period (162 and 300 h) compared to the respective reference curve in the two-phase region. Both the tests shows that the mixture didn't change its behaviour after the thermal ageing, verifying the outcomes of the previous test.

4. Transcritical power cycle performance

The performance of a simple recuperative cycle working with the $CO_2 + C_6F_6$ mixture are investigated in Aspen Plus [46]. The possibility to use a condensing cycle significantly reduces the advantages of more complex plant layout (i.e. the recompressed cycle) especially if a heavy mixture is employed [50]. The cycle is designed for a net mechanical power output of 100 MW. The analysis aims at defining the optimal mixture composition for achieving the maximum cycle efficiency.

The main assumptions for the cycle simulation are presented in Table 12. Starting from the thermal stability test results, the maximum temperature is set at 550 °C, thus coupling the power cycle with a solar tower based on commercially available molten salts [5,8]. On the other hand, the minimum cycle temperature of 51 °C is chosen in order to ensure that the mixture is in saturated liquid condition at the outlet of an air-cooled condenser in hot and arid regions ($\Delta T_{mixOUT,airIN} = 10$ °C with a maximum ambient temperature equal to 41 °C in Seville, Spain, a typical site used as European reference for CSP plants [7]). The other design parameters of the simple recuperative transcritical cycle, such as fluid machines efficiency, heat exchangers pressure drops and the minimum internal temperature approach in the recuperator, are taken in agreement with previous studies [7,23,26,27]. The pressure at the

Table 12
Assumptions for the power cycle simulations.

Parameters	units	Values
Cycle minimum temperature	°C	51
Cycle maximum temperature	°C	550
Inlet pressure of the turbine	bar	200 ÷ 350
Pump Isentropic efficiency	%	88
Expansion Isentropic Efficiency	%	92
Recuperator MITA	°C	5
DP/P Main PHE	%	2
DP/P REC HP Side	%	0.3
DP/P REC LP Side	%	1.5
DP/P Condenser	%	2

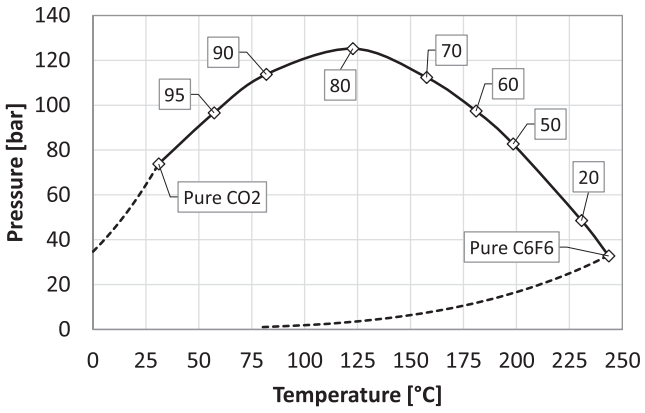

Fig. 16. CO_2-C_6F_6 mixture: Critical point locus on P-T diagram using PR EoS with Aspen Plus v11. Labels identify the critical point of the mixture with different CO_2 molar fraction. Dashed lines represent the saturation curve for the pure fluids.

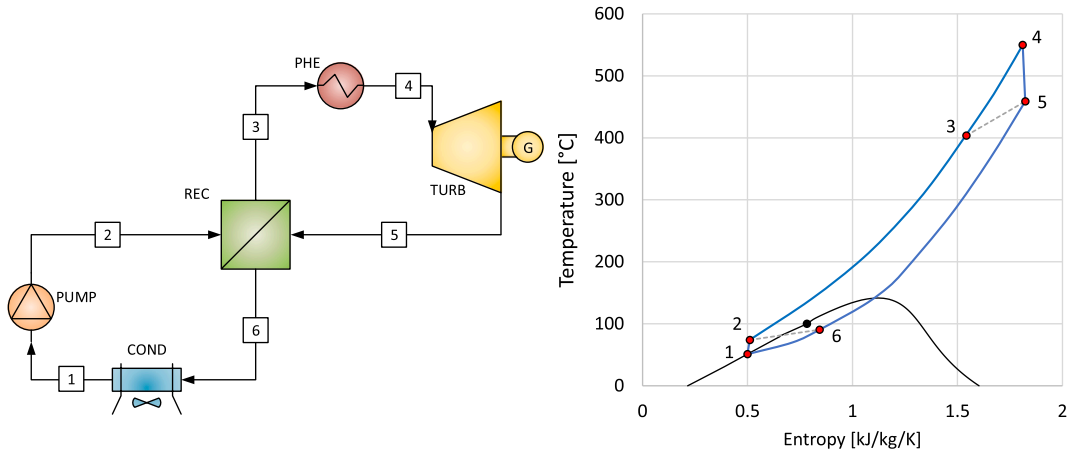

Fig. 17. Plant layout of the transcritical cycle working with CO_2 mixtures (left). Example of T-s diagrams of the simple recuperative condensing supercritical cycle for the mixture with 84% CO_2 molar content (right). The dashed lines represent the inlet–outlet conditions of the recuperative heat exchanger.

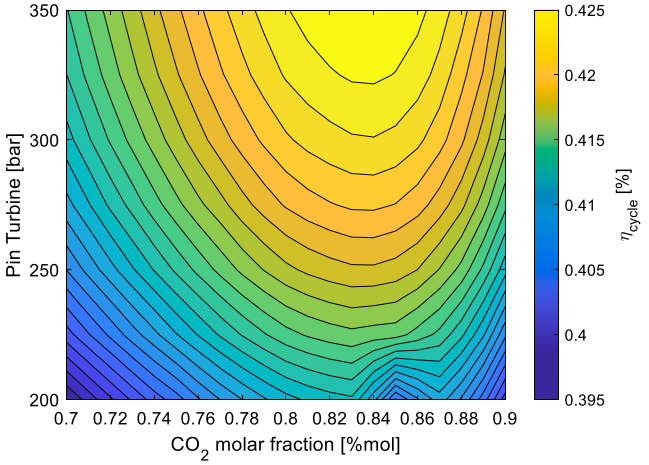

Fig. 18. Cycle efficiency as a function of the mixture molar composition and the turbine inlet pressure.

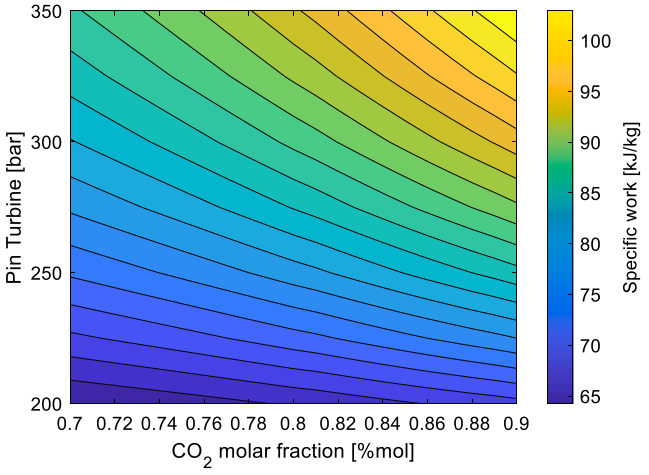

Fig. 19. Specific work as a function of the mixture molar composition and the turbine inlet pressure.

Table 13
Streams thermodynamic properties for $CO_2 + C_6F_6$ mixture with 84% CO_2 molar fraction and pure sCO2 recompressed cycle with a turbine inlet pressure of 250 bar.

Streams	CO_2 blend cycle			Pure sCO_2 recompressed cycle		
	T [°C]	P [bar]	x_{vap} [-]	T [°C]	P [bar]	x_{vap} [–]
1	51	77.7	0	51	110	1
2	72.1	255.9	0	180.3	255.9	1
3	406.4	255.1	1	419.5	255.1	1
4	550	250	1	550	250	1
5	458.0	80.6	1	454.3	115.8	1
6	90.2	79.3	0.53	185.3	112.3	1

Table 14
Cycle performance for $CO_2 + C_6F_6$ mixture with 84% CO_2 molar fraction and pure sCO2 recompressed cycle with a turbine inlet pressure of 250 bar.

Parameters	units	CO_2 blend cycle	sCO_2 recompressed
$\dot{m}$	kg/s	1232.6	1462.7
$W_{pump/comp}$	MW	25.7	54.2
Q_{rec}	MW	613.8	LT 236.3 HT 463.6
$Q_{in,PHE}$	MW	238.7	239.2
W_{turb}	MW	125.7	154.2
Q_{cond}	MW	138.7	198.4
UA_{rec}	MW/K	33.5	LT 35.1 HT 24.4
UA_{rec}/Q_{in}	1/K	0.141	0.249
η_{cycle}	%	41.9	41.8

turbine inlet is varied between 200 and 350 bar. Whereas the definition of the investigated mixture composition range depends on the power cycle application and the mixture critical point locus. Generally there are challenges related to starting the compression step close to the critical point where significant variations in thermodynamic properties introduce challenges related to system control and safe operation, particularly at off-design conditions [4,51]. So, the first criterion sets a temperature difference of 30 °C between the minimum cycle temperature (51 °C) and the critical temperature: as can be noticed in Fig. 16, this lead to a maximum CO_2 content is of 90%. On the other hand, to prevent the dopant from becoming the dominant compound in the mixture, the maximum molar fraction of the dopant was set to 30%.

The system layout, shown in Fig. 17 (left), consists of a compression step to increase the pressure of the mixture from saturated liquid conditions to the maximum cycle pressure (from 1 to 2), followed by the working fluid preheating in the recuperator (REC) (from 2 to 3), reaching the maximum cycle temperature after the primary heat exchanger (PHE) (point 4). The mixture is then expanded in the turbine (from 4 to 5) and partially cooled down in the recuperator, where it can also partially condense (from 5 to 6), before entering the condenser (COND). An example of the T-s (Temperature-Entropy) diagram for a selected mixture is reported in Fig. 17 (right).

The net thermal cycle efficiency, defined in Eq. (3), and the specific work are shown in Fig. 18 and Fig. 19 respectively at different mixture molar composition and turbine pressure inlet. This performance should be compared to the net mechanical efficiency of a traditional steam cycle, as the typical power plants applied to CSP, that is in the range of 38%-42% depending on the cold sink temperature [7,8,52]: in particular, assuming the same minimum operating temperature, it is around 38%.

$$\eta_{Cycle} = \frac{W_{Turbine} - W_{Pump}}{Q_{in,PHE}} \quad (3)$$

In general, the cycle efficiency increases with the pressure while there is an optimum value from the mixture composition point of view. A maximum efficiency of 42.4% can be found for a CO_2 content around 84% and the maximum investigated pressure of 350 bar. Anyway, moving on the optimum composition line, a 30% reduction of the pressure corresponds to a power cycle efficiency decrease of less than 0.7 percentage points. An overall techno-economic analysis can support the final choice of these two design parameters considering the fairly constant efficiency in a wide composition range and the pressure limits of the components. Concerning the cycle power balance, the higher the CO_2 content the lighter the working fluid, therefore the pump consumption and turbine output increase: this turn outs in a specific work gain at fixed operating pressure as the variation of the power produced by the turbine is higher with respect to the pump consumption in absolute terms. On the other hand, the decrease of the turbine outlet temperature leads to a reduction of the recuperator heat duty, thus increasing required input in the primary heat exchanger.

A further comparison with the state of the art pure sCO_2 recompressed cycle is made for a turbine inlet pressure of 250 bar: this operating pressure was chosen considering actual material, design and construction constraints [5]. Table 13 summarises the relevant thermodynamic properties for both the cycles. The layout of the reference pure sCO_2 cycle is represented in the Annex (Fig. A.1): the system was designed with assumptions consistent with those in Table 12 founding an optimum minimum operating pressure of 110 bar. The power balance and system performance, are then reported in Table 14. Although the efficiency values are quite similar (41.9% for the mixture vs 41.8% for the pure CO_2), the higher power consumption in the compression process for the sCO_2 cycle leads to a higher required mass flow rates and exchanged thermal power in the recuperator. In particular, the resulting UA_{PHE}/Q_{PHE} of the recuperator are 0.25 K^{-1} and 0.14 K^{-1} for the recompressed and transcritical cycle respectively, with a 14% reduction of the exchanged thermal power for the mixture, meaning that the mixture would require smaller surface areas per unit of net power. From the turbine design point of view, the expansion volumetric ratio is beneficial for the pure CO_2 cycle with a value of 2.2 compared to 3.1 of the mixture, even if the turbine power size is 22% bigger.

5. Conclusions

The exploitation of the concentrated solar power in the near future is going hand in hand with the introduction of new power block concepts for converting thermal energy into electricity. Supercritical CO_2 and transcritical CO_2 blends cycles are good candidates for the improvement of the conversion efficiency and, at the same time, the reduction of the power block complexity and size, while keeping the same reliability of the traditional steam cycle.

This work explores the adoption of $CO_2 + C_6F_6$ as working fluid in a transcritical cycle from both experimental and modelling point of view. The procedure for assessing the potentiality of the mixture consisted of three main steps. First the Vapour-Liquid equilibrium behaviour (P,x,y) was performed at three different temperatures (50, 70 and 90 °C). The experimental data, together with additional bubble points data available in literature, are then used for the calibration of the proper Equation of State. Among three selected mixture thermodynamic property models, the standard Peng-Robinson EoS is chosen using the maximum likelihood method as numerical optimization method. The PR EoS with a resulting binary interaction parameter optimised as a function of the temperature (0.163–0.000395·T [in K]) shows the lowest average mean absolute percentage error for all the investigated pressure bubble points and good results for the mixture composition at the dew points.

Secondly, the identification of the maximum mixture operating temperature through thermal stability tests was carried out. In the applied static method, the fluid sample, placed into a certain volume, is subjected to 100 h thermal stress test at gradually increasing operating temperature. The fluid degradation is then assessed by comparing the behaviour of the mixture along curves at constant specific volume (isochoric lines) before the thermal exposure and after each thermal stress tests. Results showed that even the material of the sample cylinder can have an influence on the thermal decompositions: the $CO_2 + C_6F_6$ mixture cannot withstand over 500 °C using stainless steel AISI 316L while the thermal resistance with a nickel-based alloy, Inconel 625, grew up to 600 °C.

A preliminary assessment of the power cycle was developed. The analysis aims at defining the optimal mixture composition for achieving the maximum cycle efficiency for a net mechanical power output of 100 MW. Starting from the thermal stability test results, the maximum temperature is set at 550 °C, thus coupling the power cycle with a solar tower based on commercially available molten salts. A cycle efficiency of 41.9% with a CO_2 molar content equal to 84% and a turbine inlet pressure of 250 bar was found. This value is almost 4% points higher than the performance of a traditional steam cycle while it is similar to the efficiency of a recompression pure CO_2 cycle. Anyway the transcritical cycle can rely on a simpler layout and, from a preliminary evaluation of the recuperator, the lower resulting UA_{PHE}/Q_{PHE} and the 14% reduction of the exchanged thermal power for the mixture, confirm the potentiality of the investigated mixture with respect to other configurations. A further economic analysis of both the power block and the overall CSP system is so required to prove the benefits of this solution.

CRediT authorship contribution statement

G. Di Marcoberardino: Conceptualization, Methodology, Visualization, Investigation, Software, Writing – original draft, Writing – review & editing. **E. Morosini:** Methodology, Visualization, Software, Validation, Writing – original draft, Writing – review & editing. **D. Di Bona:** Investigation, Resources, Writing – original draft. **P. Chiesa:** Methodology, Writing – review & editing, Supervision. **C. Invernizzi:** Methodology, Investigation, Writing – review & editing. **P. Iora:** Resources, Writing – review & editing, Supervision. **G. Manzolini:** Conceptualization, Project administration, Funding acquisition, Supervision.

Declaration of Competing Interest

The authors declare that they have no known competing financial interests or personal relationships that could have appeared to influence the work reported in this paper.

Table A1
Collected experimental data and uncertainties for the mixture CO2 and C6F6. The uncertainty associated with temperature measurement (with coverage factor of 2) UT is ± 0.08 K. The uncertainty associated with pressure measurement (with coverage factor of 2) UP is ± 0.005 MPa.

Point ID	T [K]	P [MPa]	x_{CO2} [–]	y_{CO2} [–]	Ux_{CO2} [–]	Uy_{CO2} [–]
1	323.15	1.031	0.1441	0.9662	± 0.0080	± 0.0044
2	323.15	2.015	0.2635	0.9812	± 0.0162	± 0.0018
3	323.15	6.996	0.7930	0.9895	± 0.0057	± 0.0007
4	323.15	8.002	0.8722	0.9873	± 0.0039	± 0.0007
5	323.15	8.502	0.9070	0.9853	± 0.0030	± 0.0008
1	343.25	1.044	0.1027	0.9286	± 0.0142	± 0.0035
2	343.25	1.500	0.1538	0.9467	± 0.0075	± 0.0024
3	343.25	2.003	0.2045	0.9572	± 0.0086	± 0.0023
4	343.25	2.530	0.2538	0.9656	± 0.0082	± 0.0018
5	343.25	3.069	0.3063	0.9681	± 0.0081	± 0.0016
6	343.25	3.509	0.3571	0.9700	± 0.0088	± 0.0015
7	343.25	4.023	0.4033	0.9728	± 0.0088	± 0.0013
8	343.25	4.520	0.4538	0.9742	± 0.0089	± 0.0012
9	343.25	5.022	0.4945	0.9747	± 0.0088	± 0.0011
10	343.25	5.525	0.5334	0.9771	± 0.0091	± 0.0010
11	343.25	6.022	0.5756	0.9763	± 0.0088	± 0.0010
12	343.25	6.601	0.6207	0.9757	± 0.0084	± 0.0010
13	343.25	6.990	0.6534	0.9758	± 0.0080	± 0.0010
14	343.25	7.500	0.6876	0.9764	± 0.0076	± 0.0009
15	343.25	8.008	0.7229	0.9746	± 0.0070	± 0.0010
16	343.25	8.644	0.7687	0.9672	± 0.0061	± 0.0012
17	343.25	9.006	0.7862	0.9633	± 0.0058	± 0.0013
18	343.25	9.453	0.8161	0.9585	± 0.0052	± 0.0014
19	343.25	9.947	0.8523	0.9564	± 0.0044	± 0.0014
20	343.25	10.467	0.8890	0.9431	± 0.0036	± 0.0018
1	363.08	0.9967	0.0698	0.8901	± 0.0039	± 0.0037
2	363.08	1.5380	0.1219	0.9320	± 0.0044	± 0.0023
3	363.08	2.0048	0.1654	0.9426	± 0.0050	± 0.0020
4	363.08	2.5620	0.2101	0.9529	± 0.0062	± 0.0018
5	363.08	3.0188	0.2542	0.9578	± 0.0065	± 0.0016
6	363.08	3.5257	0.3023	0.9619	± 0.0069	± 0.0014
7	363.08	4.0226	0.3612	0.9637	± 0.0074	± 0.0013
8	363.08	4.5158	0.3848	0.9653	± 0.0075	± 0.0012
9	363.08	5.0046	0.4341	0.9699	± 0.0077	± 0.0011
10	363.08	5.5198	0.4547	0.9682	± 0.0078	± 0.0011
11	363.08	6.0062	0.4938	0.9681	± 0.0078	± 0.0011
12	363.08	6.5633	0.5290	0.9687	± 0.0079	± 0.0011
13	363.08	7.0790	0.5596	0.9691	± 0.0078	± 0.0011
14	363.08	7.5735	0.5962	0.9672	± 0.0076	± 0.0011
15	363.08	8.0812	0.6219	0.9662	± 0.0073	± 0.0011
16	363.08	8.6014	0.6612	0.9652	± 0.0072	± 0.0013
17	363.08	9.0132	0.6913	0.9656	± 0.0068	± 0.0013
18	363.08	9.5200	0.7220	0.9574	± 0.0064	± 0.0014
19	363.08	10.0046	0.7467	0.9526	± 0.0060	± 0.0016
20	363.08	10.5056	0.7745	0.9520	± 0.0056	± 0.0016
21	363.08	11.0140	0.8116	0.9374	± 0.0049	± 0.0019
22	363.08	11.4033	0.8442	0.9199	± 0.0042	± 0.0023

Table A2
CO2 + C6F6 1st round: Vapour pressure curve: experimental measurements.

Points	T (°C)	u(T) (°C)	p (bar)	u(p) (bar)
1	20.0	1.5	11.6278	0.3003
2	40.0	1.5	12.8816	0.3000
3	60.0	1.5	14.0046	0.3001
4	80.1	1.5	15.1516	0.3001
5	100.0	1.5	16.5057	0.3004
6	120.1	1.5	17.8513	0.3012
7	130.1	1.5	18.7845	0.3009
8	140.0	1.5	19.4686	0.3021
9	150.0	1.5	20.5760	0.3008
10	160.0	1.5	21.3264	0.3004
11	170.0	1.5	21.8774	0.3001
12	180.0	1.5	22.3843	0.3001
13	190.5	1.5	22.9291	0.3000
14	200.8	1.5	23.3920	0.3000
15	210.1	1.5	23.8070	0.3000
16	220.3	1.5	24.3185	0.3011
17	230.4	1.5	24.7965	0.3000
18	240.5	1.5	25.2544	0.3000
19	250.4	1.5	25.7077	0.3000

Table A3
CO2 + C6F6 2nd round: Vapour pressure curve: experimental measurements.

Points	T (°C)	u(T) (°C)	p (bar)	u(p) (bar)
1	20.0	1.5	11.7609	0.3007
2	40.0	1.5	12.9116	0.3002
3	60.0	1.5	14.0122	0.3003
4	80.0	1.5	15.0933	0.3011
5	100.0	1.5	16.1922	0.3008
6	120.0	1.5	17.3901	0.3502
7	130.0	1.5	18.2479	0.3013
8	140.1	1.5	19.5711	0.3007
9	150.0	1.5	20.3240	0.3014
10	160.0	1.5	21.1021	0.3063
11	170.0	1.5	21.6585	0.3015
12	180.0	1.5	22.1901	0.3009
13	190.0	1.5	22.7034	0.3089

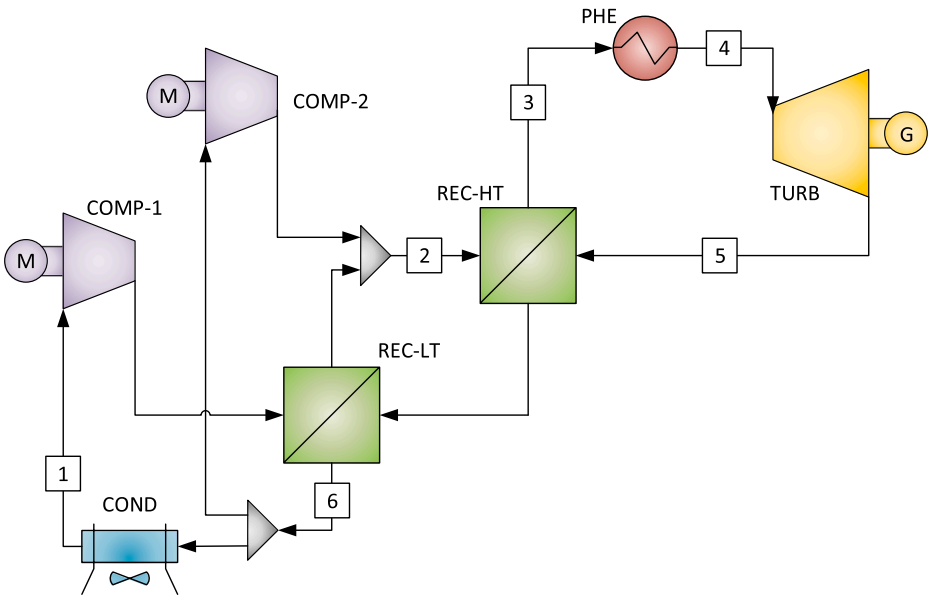

Fig. A1. Plant layout of the pure CO_2 recompressed cycle.

Acknowledgements

This paper is part of the SCARABEUS project that has received funding from the European Union's Horizon 2020 research and innovation programme under grant agreement No 814985.

Appendix A

See Tables A1-A3 and Fig. A1.

References

[1] M.T. Dunham, B.D. Iverson, High-efficiency thermodynamic power cycles for concentrated solar power systems, Renew. Sustain. Energy Rev. 30 (2014) 758–770, https://doi.org/10.1016/j.rser.2013.11.010.
[2] F. Crespi, D. Sánchez, J.M. Rodríguez, G. Gavagnin, A thermo-economic methodology to select sCO2 power cycles for CSP applications, Renew. Energy. 147 (2020) 2905–2912, https://doi.org/10.1016/j.renene.2018.08.023.
[3] M. Binotti, M. Astolfi, S. Campanari, G. Manzolini, P. Silva, Preliminary assessment of sCO2 cycles for power generation in CSP solar tower plants, Appl. Energy 204 (2017) 1007–1017, https://doi.org/10.1016/j.apenergy.2017.05.121.
[4] M.T. White, G. Bianchi, L. Chai, S.A. Tassou, A.I. Sayma, Review of supercritical CO2 technologies and systems for power generation, Appl. Therm. Eng. 185 (2021), 116447, https://doi.org/10.1016/j.applthermaleng.2020.116447.
[5] C.K. Ho, M. Carlson, P. Garg, P. Kumar, Technoeconomic Analysis of Alternative Solarized s-CO2 Brayton Cycle Configurations, J. Sol. Energy Eng. 138 (2016), https://doi.org/10.1115/1.4033573.
[6] F. Crespi, D. Sánchez, T. Sánchez, G.S. Martínez, S. David, G.S. Mart, Capital Cost Assessment of Concentrated Solar Power Plants Based on Supercritical Carbon Dioxide Power Cycles, J. Eng. Gas Turbines Power 141 (2019), https://doi.org/10.1115/1.4042304.
[7] M. Binotti, C.M. Invernizzi, P. Iora, G. Manzolini, Dinitrogen tetroxide and carbon dioxide mixtures as working fluids in solar tower plants, Sol. Energy 181 (2019) 203–213, https://doi.org/10.1016/j.solener.2019.01.079.
[8] S. Polimeni, M. Binotti, L. Moretti, G. Manzolini, Comparison of sodium and KCl-MgCl2 as heat transfer fluids in CSP solar tower with sCO2 power cycles, Sol. Energy 162 (2018) 510–524, https://doi.org/10.1016/j.solener.2018.01.046.
[9] SCARABEUS, Supercritical Carbon dioxide/Alternative fluids Blends for Efficiency Upgrade of Solar power plants, (2019). https://www.scarabeusproject.eu/ (accessed 31 March 2022).
[10] DESOLINATION, DEmonstration of concentrated SOLar power coupled wIth advaNced desAlinaTion system in the gulf regION, (2021). https://cordis.europa.eu/project/id/101022686 (accessed on 31 March 2022).
[11] COMPASsCO2: COMponents' and Materials' Performance for Advanced Solar Supercritical CO2 Power Plants, (n.d.). https://cordis.europa.eu/project/id/958418 (accessed on 31 March 2022).
[12] sCO2-Flex: Supercritical CO2 Cycle for Flexible and Sustainable Support to the Electricity System, (n.d.). https://cordis.europa.eu/project/id/764690 (accessed on 31 March 2022).
[13] sCO2-Hero: The Supercritical CO2 Heat Removal System, (n.d.). https://cordis.europa.eu/ project/id/662116 (accessed on 31 March 2022).
[14] CO2OLHEAT: Supercritical CO2 Power Cycles Demonstration in Operational Environment Locally Valorising Industrial Waste Heat, (n.d.). cordis.europa.eu/project/id/101022831 (accessed on 31 March%0A2022).
[15] S.A. Wright, T.M. Conboy, G.E. Rochau, Break-even Power Transients for two Simple Recuperated S-CO 2 Brayton Cycle Test Configurations, SCO2 Power Cycle Symp. (2011) 1–31.
[16] Y. Ahn, J. Lee, S.G. Kim, J.I. Lee, J.E. Cha, S.-W. Lee, Design consideration of supercritical CO2 power cycle integral experiment loop, Energy. 86 (2015) 115–127, https://doi.org/10.1016/j.energy.2015.03.066.
[17] T.C. Allison, J. Jeffrey Moore, D. Hofer, M.D. Towler, J. Thorp, Planning for Successful Transients and Trips in a 1 MWe-Scale High-Temperature sCO2 Test Loop, J. Eng. Gas Turbines Power 141 (2019), https://doi.org/10.1115/1.4041921.
[18] J. Marion, M. Kutin, A. McClung, J. Mortzheim, R. Ames, The STEP 10 MWe sCO2 Pilot Plant Demonstration, ASME Turbo Expo 2019 Turbomach, Tech. Conf. Expo. (2019), https://doi.org/10.1115/GT2019-91917.
[19] Y. Le Moullec, Z. Qi, J. Zhang, P. Zhou, Z. Yang, X. Wang, W. Chen, S. Wang, 2019 3rd European supercritical CO2 Conference September 19-20 Paris, France, Shouhang-EDF 10MWe supercritical CO2 cycle + CSP demonstration project, 3rd Eur. Conf. Supercrit. CO2 Power Syst. 2019 19th-20th Sept. 2019. (2019) 138–147. https://doi.org/10.17185/duepublico/48884.
[20] M. Atif, F.A. Al-Sulaiman, Energy and exergy analyses of solar tower power plant driven supercritical carbon dioxide recompression cycles for six different locations, Renew. Sustain. Energy Rev. 68 (2017) 153–167, https://doi.org/10.1016/j.rser.2016.09.122.
[21] C. Invernizzi, Prospects of Mixtures as Working Fluids in Real-Gas Brayton Cycles, Energies. 10 (2017) 1649, https://doi.org/10.3390/en10101649.
[22] C.M. Invernizzi, P. Iora, D. Bonalumi, E. Macchi, R. Roberto, M. Caldera, Titanium tetrachloride as novel working fluid for high temperature Rankine Cycles: Thermodynamic analysis and experimental assessment of the thermal stability, Appl. Therm. Eng. 107 (2016) 21–27, https://doi.org/10.1016/J.APPLTHERMALENG.2016.06.136.
[23] F. Crespi, G.S. Martínez, P.R. De Arriba, D. Sánchez, F. Jiménez-Espadafor, Influence of working fluid composition on the optimum characteristics of blended supercritical carbon dioxide cycles, Proc. ASME Turbo Expo. 10 (2021) 1–11, https://doi.org/10.1115/GT2021-60293.
[24] G. Di Marcoberardino, C.M. Invernizzi, P. Iora, A. Ayub, D. Di Bona, P. Chiesa, M. Binotti, G. Manzolini, Experimental and analytical procedure for the characterization of innovative working fluids for power plants applications, Appl. Therm. Eng. 178 (2020), 115513, https://doi.org/10.1016/j.applthermaleng.2020.115513.
[25] S. Lasala, C. Invernizzi, P. Iora, P. Chiesa, E. Macchi, Thermal Stability Analysis of Perfluorohexane, Energy Procedia (2015) 1575–1582, https://doi.org/10.1016/j.egypro.2015.07.358.
[26] G. Di Marcoberardino, E. Morosini, G. Manzolini, Preliminary investigation of the influence of equations of state on the performance of CO2 + C6F6 as innovative working fluid in transcritical cycles, Energy. 238 (2022), 121815, https://doi.org/10.1016/j.energy.2021.121815.
[27] O.A. Aqel, M.T. White, M.A. Khader, A.I. Sayma, Sensitivity of transcritical cycle and turbine design to dopant fraction in CO2-based working fluids, Appl. Therm. Eng. 190 (2021), 116796, https://doi.org/10.1016/j.applthermaleng.2021.116796.

[28] C.M. Colina, A. Galindo, F.J. Blas, K.E. Gubbins, Phase behavior of carbon dioxide mixtures with n-alkanes and n-perfluoroalkanes,, Fluid Phase Equilib. (2004) 77–85, https://doi.org/10.1016/j.fluid.2004.06.021.
[29] L.R. Dinanno, F.A. Dibella, M.D. Koplow, An RC-1 Organic Rankine Bottoming Cycle for an Adiabatic Diesel Engine, 1983.
[30] David M. Lemal, Perspective on Fluorocarbon Chemistry, J. Org. Chem. 69 (1) (2004) 1–11, https://doi.org/10.1021/jo0302556.
[31] S. Lasala, D. Bonalumi, E. Macchi, R. Privat, J.N. Jaubert, The design of CO2-based working fluids for high-temperature heat source power cycles, Energy Procedia 129 (2017) 947–954, https://doi.org/10.1016/j.egypro.2017.09.125.
[32] W.L. Fielder, Thermal decomposition of some linear perfluoroalkanes in an Inconel bomb, NASA, Technical Note D-1744, Lewis Research Center, Cleveland, Ohio, 1963.
[33] Ø. Hodnebrog, B. Aamaas, J.S. Fuglestvedt, G. Marston, G. Myhre, C.J. Nielsen, M. Sandstad, K.P. Shine, T.J. Wallington, Wallington, Updated Global Warming Potentials and Radiative Efficiencies of Halocarbons and Other Weak Atmospheric Absorbers, Rev. Geophys. 58 (3) (2020), https://doi.org/10.1029/2019RG000691.
[34] E.M.S. Lasala, P. Chiesa, Binary mixtures of carbon dioxide and fluorocarbons as working fluids for power production applications, in: Conf. Proc. JEEP2014 – 40ième Journées d'Etudes Des Equilibres Entre Phases, Lyon, France, 2014.
[35] Joseph M. Antonucci, Leo A. Wall, High-Temperature Reactions of Hexafluorobenzene, J. Res. Notional Bur. Stand. - A. Phys. Chem. 70A (6) (1966) 473, https://doi.org/10.6028/jres.070A.041.
[36] A.M.A. Dias, J.L. Daridon, J.C. Pa, Vapor - Liquid Equilibrium of Carbon Dioxide - Perfluoroalkane Mixtures : Experimental Data and SAFT Modeling, Ind. Eng. Chem. Res. 45 (2006) 2341–2350.
[37] LEAP Scarl, LEAP Website. (2022). https://www.leap.polimi.it/ (accessed 31 March 2022).
[38] Fluid Test Laboratory, Università degli Studi di Brescia, (2022). http://www.gecos.polimi.it/laboratories/brescia/ (accessed 31 March 2022).
[39] Silvia Lasala, Paolo Chiesa, Daniele Di Bona, Stefano Consonni, Vapour - Liquid Equilibrium measurements of CO2-based mixtures: Experimental apparatus and testing procedures, Energy Procedia 45 (2014) 1215–1224, https://doi.org/10.1016/j.egypro.2014.01.127.
[40] S.A. Gornati, D. Di Bona, P. Chiesa, New experimental VLE data for the binary mixture of carbon dioxide + perfluorohexane (CO2 + C6F14) from 273 K to 333 K, Fluid Phase Equilib. 498 (2019) 94–103, https://doi.org/10.1016/j.fluid.2019.06.024.
[41] Ralf Dohrn, Stephanie Peper, José M.S. Fonseca, High-pressure fluid-phase equilibria: Experimental methods and systems investigated (2000–2004), Fluid Phase Equilib. 288 (1-2) (2010) 1–54, https://doi.org/10.1016/j.fluid.2009.08.008.
[42] Silvia Lasala, Paolo Chiesa, Romain Privat, Jean-Noël Jaubert, Sizing and operating units for the purification and compression of CO2-based streams: The impact of thermodynamic model accuracy, J. Supercrit. Fluids 140 (2018) 336–347, https://doi.org/10.1016/j.supflu.2018.04.010.
[43] NIST - National Institute of Standards and Technology, REFPROP - Reference Fluid Thermodynamic and Transport Properties, (n.d.). https://www.nist.gov/srd/refprop (accessed 31 March 2022).
[44] Ana M.A. Dias, Carla M.B. Gonçalves, Ana I. Caço, Luís M.N.B.F. Santos, Manuel M. Piñeiro, Lourdes F. Vega, João A.P. Coutinho, Isabel M. Marrucho, Densities and vapor pressures of highly fluorinated compounds, J. Chem. Eng. Data 50 (4) (2005) 1328–1333, https://doi.org/10.1021/je050056e.
[45] Silvia Lasala, Paolo Chiesa, Romain Privat, Jean-Noël Jaubert, VLE properties of CO2 – Based binary systems containing N2, O2 and Ar: Experimental measurements and modelling results with advanced cubic equations of state, Fluid Phase Equilib. 428 (2016) 18–31, https://doi.org/10.1016/j.fluid.2016.05.015.
[46] AspenTech, Aspen Plus, (2022). http://www.aspentech.com/products/aspen-plus.aspx (accessed 31 March 2022).
[47] International ASTM, ASTM D6743-11, Standard Test Method for Thermal Stability of Organic Heat Transfer Fluids, West Conshohocken, PA, 2011. www.astm.org.
[48] Officine Orsi, (2022). https://www.officineorsi.com/index.php (accessed 31 March 2022).
[49] Marco Pasetti, Costante M. Invernizzi, Paolo Iora, Thermal stability of working fluids for organic Rankine cycles: An improved survey method and experimental results for cyclopentane, isopentane and n-butane, Appl. Therm. Eng. 73 (1) (2014) 764–774, https://doi.org/10.1016/j.applthermaleng.2014.08.017.
[50] G. Manzolini, M. Binotti, D. Bonalumi, C. Invernizzi, P. Iora, CO2 mixtures as innovative working fluid in power cycles applied to solar plants. Techno-economic assessment, Sol. Energy 181 (2019) 530–544, https://doi.org/10.1016/J.SOLENER.2019.01.015.
[51] S.S. Saravi, S.A. Tassou, An investigation into sCO2 compressor performance prediction in the supercritical region for power systems, Energy Procedia (2019) 403–411, https://doi.org/10.1016/j.egypro.2019.02.098.
[52] B. Kelly, M. Izygon, L. Vant-Hull, Advanced Thermal Energy Storage for Central Receivers with supercritical coolants, SolarPaces Conf. (2010), https://doi.org/10.2172/981926.